AD-A172 154 SPECTROPHONE MEASUREMENTS IN SULFUR HEXAFLUORIDE(U) 1/1
MISSISSIPPI UNIV UNIVERSITY PHYSICAL ACOUSTICS RESEARCH
LAB H E BASS ET AL. 01 OCT 85 PARCUM-85-06
UNCLASSIFIED N00014-84-C-0193 F/G 7/4 NL

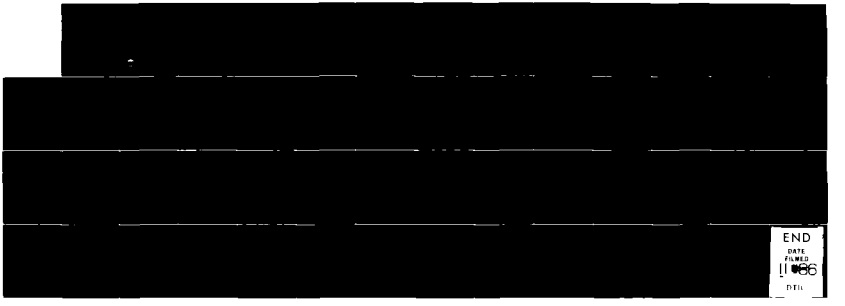

END
DATE FILMED
11 86
DTIC

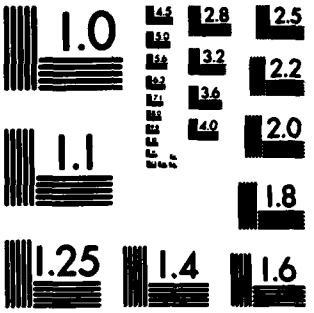

SPECTROPHONE MEASUREMENTS IN SULFUR HEXAFLUORIDE

Henry E. Bass and Manaf H. Ali

PARGUM 85-06

THE UNIVERSITY OF MISSISSIPPI
PHYSICAL ACOUSTICS RESEARCH GROUP
DEPARTMENT OF PHYSICS AND ASTRONOMY

Unclassified

SECURITY CLASSIFICATION OF THIS PAGE (When Data Entered) AD-A172 154

REPORT DOCUMENTATION PAGE

READ INSTRUCTIONS BEFORE COMPLETING FORM

1. REPORT NUMBER: PARGUM 85-06	2. GOVT ACCESSION NO.: N/S
3. RECIPIENT'S CATALOG NUMBER: N/A	
4. TITLE (and Subtitle): Spectrophone Measurements in Sulfur Hexafluoride	5. TYPE OF REPORT & PERIOD COVERED:
6. PERFORMING ORG. REPORT NUMBER: PARGUM 85-06	
7. AUTHOR(s): Henry E. Bass and Manaf H. Ali	8. CONTRACT OR GRANT NUMBER(s): N000114-84-C-0193
9. PERFORMING ORGANIZATION NAME AND ADDRESS: Physical Acoustics Research Laboratory, Department of Physics and Astronomy, The University of Mississippi; Univ., MS 38677	10. PROGRAM ELEMENT, PROJECT, TASK AREA & WORK UNIT NUMBERS: 61153N, RR011-08-01, NR 384-936
11. CONTROLLING OFFICE NAME AND ADDRESS: Office of Naval Research, 206 O'Keefe Building, Atlanta, GA 30332	12. REPORT DATE: 1 Oct 85
	13. NUMBER OF PAGES: 50
14. MONITORING AGENCY NAME & ADDRESS (if different from Controlling Office)	15. SECURITY CLASS. (of this report): Unclassified
	15a. DECLASSIFICATION/DOWNGRADING SCHEDULE

16. DISTRIBUTION STATEMENT (of this Report)

Approved for public release; distribution unlimited.

17. DISTRIBUTION STATEMENT (of the abstract entered in Block 20, if different from Report)

N/A

18. SUPPLEMENTARY NOTES

The view, opinions, and/or findings contained in this report are those of the author(s) and should not be construed as an official Office of Naval Research position, policy, or decision, unless so designated by other documentation.

19. KEY WORDS (Continue on reverse side if necessary and identify by block number)

Optoacoustic Effect, Sulfur Hexafluoride, Vibrational Energy Transfer, Spectrophone

20. ABSTRACT (Continue on reverse side if necessary and identify by block number)

Short pulses (~1 μs) of 10.6 radiation from a CO_2 laser have been used to generate optoacoustic pulses in gaseous SF_6. The optical path length for 10.6 radiation in SF_6 is very short at intermediate pressures (~1 Torr) so a strong acoustic pulse is generated which travels in the direction of the incident laser beam (in addition to cylindrical expansion). As the gas pressure is decreased, the optical path length increases resulting in an acoustic pulse with a shape dominated by collisional transfer in SF_6. As the pressure is lowered further (~200 mTorr), thermal conduction to the test cell walls and spontaneous radia-

DD FORM 1 JAN 73 1473 EDITION OF 1 NOV 65 IS OBSOLETE S/N 0102-014-6601

Unclassified

SECURITY CLASSIFICATION OF THIS PAGE (When Data Enter

tion by the excited gas become important. As these mechanisms begin to compete with slow collisional energy transfer processes, the optoacoustic signal changes in sign. A microscopic description of the behavior is included. Keywords: Vibrational Energy Transfer

SPECTROPHONE MEASUREMENTS IN SULFUR HEXAFLUORIDE

Henry E. Bass and Manaf H. Ali

PARGUM 85-06

FOREWORD

This report is an adaptation of Manaf Hassan Ali's Ph.D. dissertation, "Spectrophone Measurements in Sulfur Hexafluoride," which was accepted by the faculty of the Department of Physics and Astronomy at the University of Mississippi on September 10, 1985. The work reported was carried out at the University of Mississippi's Physical Acoustics Research Laboratory with support from the Office of Naval Research.

Henry E. Bass
Dissertation Director

LIST OF TABLES

Page

Table

LIST OF FIGURES

CHAPTER 1

Introduction

Alexander Graham Bell (1880)[1] observed that audible sound can be produced by exposing a gas in a constant volume container to intensity modulated infra-red radiation. He explained that part of the radiation is absorbed by the gas raising the temperature and hence pressure in the constant-volume enclosure. A periodic modulation of the incident intensity thus produces an alternating pressure component which becomes audible for proper choices of the experimental parameters. Bell realized the possibility of using the effect to investigate the absorption spectra of gases. He proposed the name "spectrophone" for the instrument constructed for this purpose.

With the advent of molecular theory[2] this process was interpreted in detail. When molecules absorb infra-red radiation, the energy taken up appears as quanta of vibrational energy. A molecule may lose this energy by spontaneous emission of radiation, by induced emission, or by transfer of energy to thermal energy of motion. This last process occurs in collisions when the vibrational energy is transferred to translation. An increase in translational energy means the gas will heat and reach a new temperature. If the gas is illuminated by infra-red radiation which is periodically interrupted, it will heat and cool, and a periodic change of pressure will be observed in a constant volume system. These periodic

pressure changes lead to sound emission which can be detected by means of a microphone.

Interest in the spectrophone has increased after the experimental tools applied for investigation of molecular energy transfer in gases shifted from pure thermodynamic ones to optical methods. Part of this interest is because the spectrophone proves to be a powerful tool to measure relaxation rates. Early spectrophone measurements of vibrational relaxation used a light source modulated to be nearly sinusoidal in amplitude with a variable frequency. The time required to transfer energy from the excited vibrational state to translation was measured as either frequency dependent phase shift or signal amplitude. Filtered radiation can be used so that for polyatomic molecules the relaxation time for individual vibrational modes can be studied separately. Gorelik[3] pointed out that if there is a time lag between the absorption of a vibrational quantum and its degradation to thermal energy, it should determine a phase difference between the modulation of the incident radiation and the emitted sound wave. This phase shift is then a function of the relaxation time of the vibrational level. Also the amplitude of the sound wave is a function of the relaxation time of the absorbing level.

Modern measurements employ either modulated or pulsed light. Measurements of vibrational energy transfer using an amplitude modulated laser beam and phase sensitive detection[4] have been most common and have provided a great deal of information about the details of energy transfer. The pressure response following illumination depends in

magnitude (and direction) on the amount of energy transferred to or from translation. This feature provides the spectrophone with a unique capability to determine energy transfer pathways.

The pulsed spectrophone[5] offers certain advantages over the continuously modulated configuration. One major advantage is the ability to delay interference from cell resonances by varying the cell length. An additional advantage is that the amplitude and time evolution are measured as separate quantities at the same time (during a single shot) rather than measuring the phase shift between modulated excitation and pressure response as a function of frequency. This feature[6] requires that the microphone and electronics used in the pulsed spectrophone have a large bandwidth.

Interpretation of spectrophone data requires accurate relations between the microscopic energy transfer processes and the measured pressure variation as well as a description of other macroscopic processes which affect the signal, e.g., acoustic propagation and thermal conduction. Bauer[7] has developed a general theory for relating the microscopic energy transfer processes to the opto-acoustic response for a gas with multiple internal energy levels. Basically, using his approach, one must assume a set of energy transfer rates and a reaction scheme, then compute the predicted response. The resulting pressure evolution is compared to experiment and the rates and reaction scheme are adjusted until agreement is achieved. There is no assurance, of course, that the resultant rates and reaction scheme are unique. This is true of other

methods used to measure vibrational relaxation times as well, e.g., time resolved laser induced fluorescence and ultrasonic absorption and dispersion. One major strength of his generalized approach is that the same procedure can simultaneously compute sound absorption curves and laser fluorescence decay times for the assumed reaction scheme. By comparing the predictions to sound absorption, laser fluorescence, and spectrophone data at the same time, some reaction schemes can be eliminated. The reaction scheme which gives results in agreement with all three experiments is still not, necessarily, unique, but at least it will be consistent with all available data.

In this work a pulsed spectrophone has been used to determine its applicability to measure relaxation rates in a polyatomic gas. The SF_6 molecular system was chosen as a test case because energy transfer in SF_6 has been thoroughly studied using other techniques and it strongly absorbs CO_2 laser radiation. Data available from other techniques[2,8,9] will enable us to eliminate reaction schemes inconsistent with other techniques.

The objective of this work was to develop a method to solve the kinetic equations for the spectrophone response including spontaneous emission and acoustic effects as a function of time and to test the solution experimentally. This objective has been achieved by solving the heat equation for the gas inside the cell by numerical integration.

CHAPTER 2

Description of Experiment

A block diagram of the experimental apparatus is shown in Figure 1. The apparatus consists of a source of pulsed IR radiation, a test cell, a microphone and preamplifier, signal averaging, and gas handling equipment.

IR Source

The IR source is a CO_2 laser consisting of a 2.5 cm i.d. glass tube, 125 cm long sealed with sodium chloride (index of refraction 1.46 at 10.6μ) windows mounted at the Brewster's angle of 56°, and two aluminum coated mirrors. A mixture of 11% CO_2, 8% N_2 and 81% He (Matheson, Co. premixed) flows in at one end. An electric discharge through the gas mixture is maintained by a continuous D.C. power supply operating at about 7kV and 20 mA. The CO_2-N_2-He mixture is pumped out of the tube at the other end. The continuous flow serves to cool the laser gas and helps to remove impurities and vibrationally excited gas which might decrease the laser efficiency. Further cooling of the laser gas is provided by thermal conduction through the tube walls to a surrounding water jacket. Pressure inside the laser tube was generally 6-10 torr. The CO_2 laser is Q-switched with a rotating mirror which is mounted on a D.C. motor to deliver pulses approximately 1 μs in duration. Mirror M_1 is the output mirror and is coated for 20% transmission at 10.6 μm. The

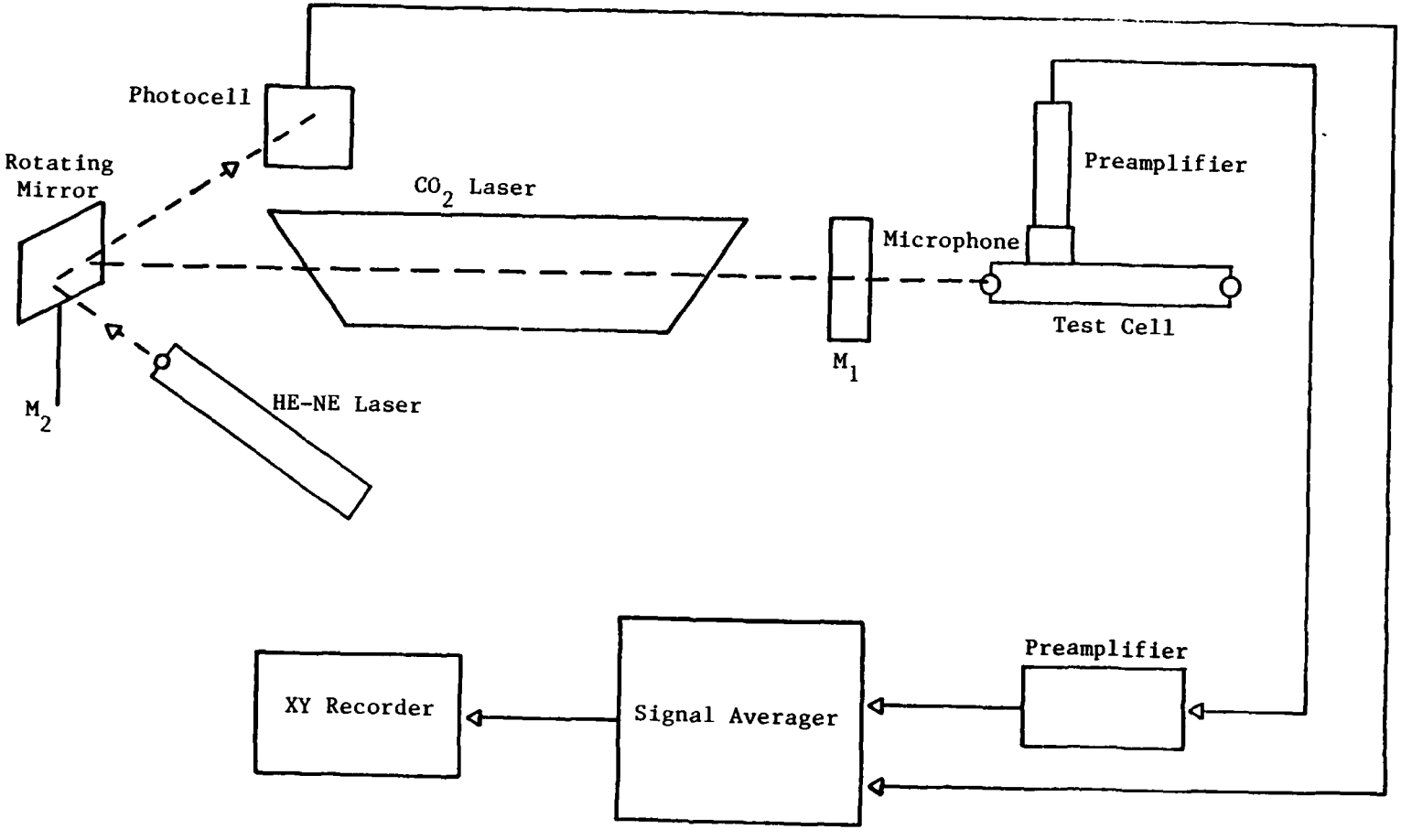

Figure 1. Block Diagram of the Experimental Apparatus.

laser is capable of delivering approximately 1 W of 10.6μm radiation when operated in a continuous mode.

Associated with the laser is a triggering circuit used to initiate the electronics. This circuit consists of a 1 mW He/Ne laser and a box containing a photodiode cell, amplifier chip, and a logic circuit. The power to the circuit was provided by a 9V battery. The He/Ne laser is directed into Mirror M_2 so that just before M_2 rotates into a position to close the laser cavity, the He/Ne beam strikes the photodiode which provides a pulse. After amplifying the pulse with an amplifier chip and shaping it by the logic circuit to give a 5V square wave, it was used to trigger the signal averager.

Test Cell

The body of the cell is a tube mounted so that its axis is coincident with the laser tube axis, and hence the laser beam axis. The characteristics of the test cell are a strong function of the particular system to be studied. Cylindrical geometry seems natural due to the approximately cylindrical beam shape. The length of the test cell is chosen to be 50 cm long. Selection of the cell radius is influenced by several interdependent considerations. Across the cell radius, the gas is illuminated uniformally and the pressure evolution occurs simultaneously. The microphone, however, is located in the side of the test cell so it responds to pressure changes at the cell center after a time $\frac{r}{c}$ where r is the cell radius and c is the speed of sound in the gas.

The resulting pressure response, then, will be averaged over a time $\frac{r}{c}$ and any processes with a shorter time constant will not be distinguished clearly. For SF_6, $c \cong 100$ m/sec so in order to observe a 20 μsec relaxation time, r must be less than 2 mm. Transit time considerations argue for a small r. When the radius is decreased, however, thermal conduction becomes more important. The characteristic time for thermal conduction τ_{tc}, decreases as r^2. If τ_{tc} is much less than the slowest relaxation process of interest, that slow process will be difficult to observe. The final consideration is the magnitude of the pressure response. In order to avoid multiphoton processes, the laser intensity cannot be increased indefinitely. As the cell cross section decreases, then, the signal amplitude will decrease.

We selected a 50 cm long test cell with radius of 2 mm. The cell is approximately cylindrical with salt flats on both ends. The microphone is mounted in the side of the test cell near the entrance window. The microphone extends slightly into the 2 mm cylinder so the effective radius at the microphone location is less than 2 mm, perhaps 1 mm from beam center to the nearest part of the microphone face. Gas inlets are provided near each end of the cell so that the cell can be flushed with the gas of interest. Also connected directly to the test cell are the pressure transducers.

Microphone

The microphone is very important for the measurements. The response of the microphone can affect the recorded pressure response. The microphone response, at low frequencies, is determined by leakage of air

from front to back of the diaphragm. At high frequencies, the diaphragm begins to oscillate in a resonant mode. For pulsed measurements, the microphone must be broad-band with an upper frequency limit $f_u >> 1/(2\pi\tau)$ where τ is the fastest relaxation process of interest. For our purpose f_u should be greater than 20 kHz. This condition is easily achieved with modern capacitance microphones.

A standard commercial capacitance microphone has an air gap between a backing plate and a metal diaphragm which forms the pressure sensitive capacitance. These microphones rely on this air gap to damp the diaphragm motion and, as a result, quite often ring when hit by a short pulse at low pressure. For this reason, we used a solid dielectric capacitance microphone with an upper frequency limit of approximately 100 kHz.[6]

The low frequency microphone response was measured using a substitution technique with a B&K 4149 microphone as the standard. The speaker used as a source consisted of a 16 inch diameter driver mounted in a 725 liter box giving a frequency response of 50-5000 Hz. The electrical source was taken from an HP 3561A dynamic signal analyzer. The analyzer generates band limited noise then Fourier analyzes the input signal. The signal from the reference microphone is stored and subtracted from the signal from the microphone under test. Results of the calibration procedure are shown as Figure 2. Note that no effort was made to define the high frequency cut off of the test microphone. We did determine that this cut off was above that of our reference microphone (30 kHz). Since the microphone relies on gas in pockets between the dielectric membrane

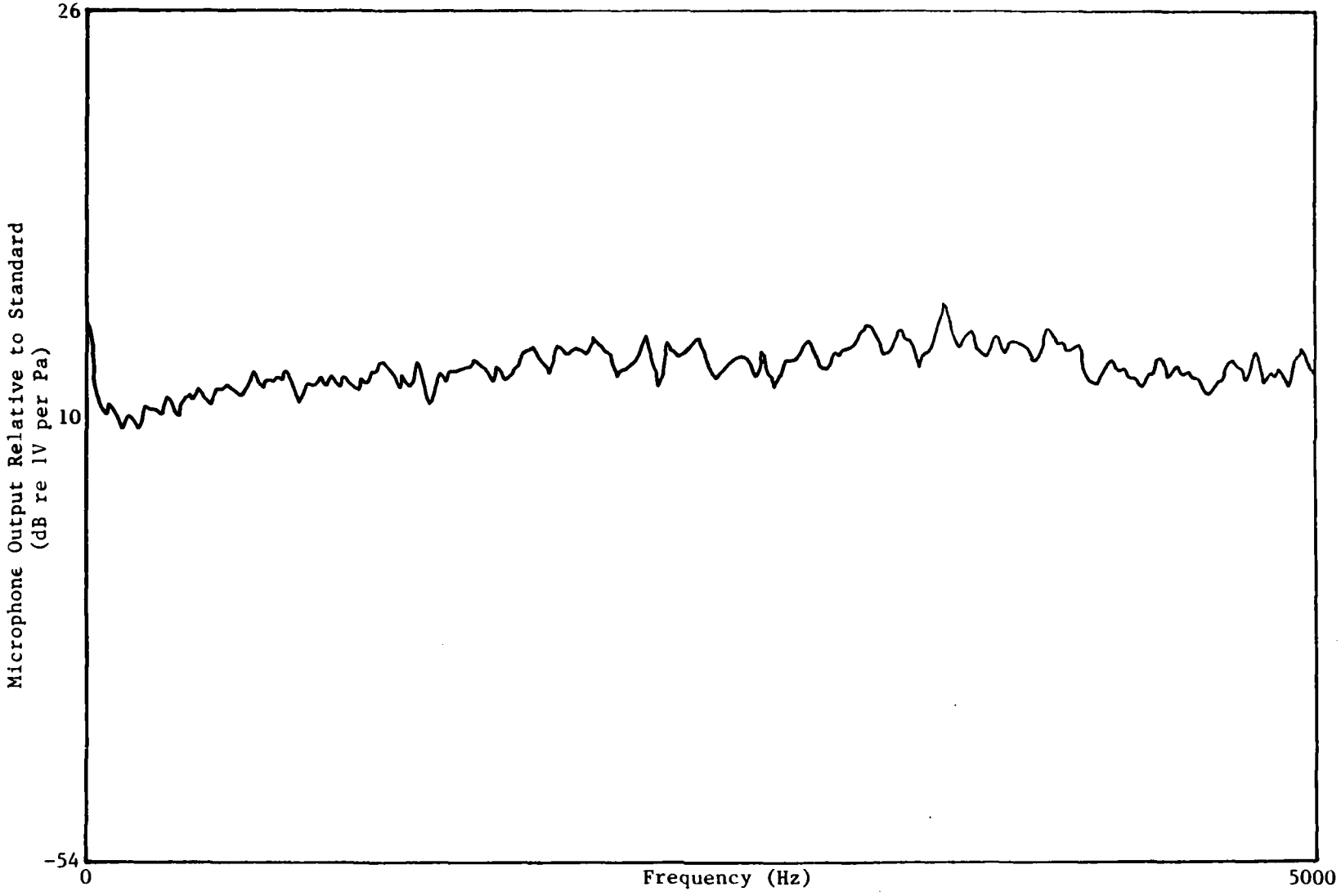

Figure 2. The Microphone Response.

and the backing plate, the sensitivity decreases slightly with lower pressure, but the loss in sensitivity is much more acceptable than ringing.

The microphone signal was preamplified first with a General Radio type 1560-42 preamplifier specifically designed to amplify the output from a capacitive source. The preamplifier offers a gain of either X1 or X10. A self-contained oscillator/rectifier circuit supplies the polarizing voltage (+200V) for air-condenser microphones. The signal was preamplified again with an EG&G PARC Model 113 preamplifier. Amplifiers were flat within 3 dB from below 7 Hz to above 200 kHz. Total gain was typically 10^4.

Signal Averager

The preamplified microphone signal was averaged with a Honeywell/Saicor averager. Its function when operated in the signal enhancement mode is to provide detection and enhancement of a periodic or periodically stimulated signal buried in noise or other disturbance through an averaging procedure which preserves the wave shape of the signal while averaging out non-coherent noise. The waveform is divided into 400 points with resolution (or spacing between points) selectable from 0.2 μsec to 1 sec. From 2^9 to 2^{17} (in binary steps) successive cycles can be linearly averaged in addition to the continuous operation mode. The averager was triggered externally by the He/Ne laser reflected from the rotating mirror which Q-switched the CO_2 laser. The output S/N is typically less than one so the signal cannot be viewed on an oscilloscope except at high pressure. The signal averager was operated either

in the clipped or full mode depending upon S/N ratio. The output from the averager was sent to an X-Y recorder for a permanent record.

Gas Handling Equipment

The SF_6 gas used was supplied by Matheson with a stated purity of 99.98%. To keep water vapor from leakage and outgassing low, the gas cell was evacuated for several days prior to measurements. The combined leak/outgassing rate was 0.3 mtorr/min. Pressures were measured with MKS Baratron tranducers type 220. The transducers were factory calibrated and certified for 0.1 percent accuracy.

The experiment consists of turning on the laser and the rotating mirror to Q-switch the laser and adjusting the mirrors to get radiation of maximum energy. Energy was measured with a pyroelectric energy meter to be ~20 μJ/pulse. Then the cell was filled with SF_6 gas to the maximum desired pressure of measurement ~1000 mtorr. Next the cell was illuminated with IR radiation from the laser. The test cell had IR windows on both ends to allow the laser beam to enter and exit.

The acoustic signal was picked up by the microphone which was mounted in the cell wall near the entrance. At the same time the He/Ne laser was turned on to initiate the triggering of the signal averager. After the signal had passed through the preamplifier and signal averager, it was recorded on the X-Y recorder. The pressure in the test cell was then lowered to the next desired pressure and another run was made. To avoid accumulation of water vapor, the test cell was evacuated every three runs. This continued until the desired pressure range had been covered.

CHAPTER 3

Theory

In 1972, Bauer[7] published a theory for the spectrophone response results from collisional energy transfer using a matrix notation which is well adapted to numerical calculation. Thermodynamic conditions are assumed to be adiabatic. Bauer assumed the system was perturbed by optical transitions then the resulting collisional transitions were considered. The collisional change of the population numbers determines the amount of energy exchanged between the translational and internal degrees of freedom. When applying the theory to a multilevel gas, Bauer pointed out that application of linear algebra allows one to represent the matrices by their eigen-properties which leads to a decomposition of the optoacoustic response into single relaxation terms.

The main steps of Bauer's development will be used here to derive the temperature response resulting from absorbed radiation (for more information cf. Ref. 7). Bauer considered multiple optical transitions as well as collisional transitions.

Collision processes refer to transferring vibrational energy from one mode to another or to translation. Thermal conduction is also a result of energy transfer during collisions but for the purpose of this dissertation thermal conduction will not be included in the term collisional processes. Thermal conduction will be treated separately.

Optical Transition

Consider one optical transition which takes a molecule of type M in state k (denoted M_k) to state i by addition of a quantum of radiation

with frequency ν_{ik}. The reaction can be written as

$$M_i \rightleftarrows M_k + h\nu_{ik} \tag{1}$$

The rate of change of occupation numbers (n_i for population of M_i and $_k$ for population of M_k) due to absorption and stimulated emission can be written as

$$\dot{n}_i = \nu_{ik}(B_{ki}n_k - B_{ik}n_i) \tag{2}$$

where B_{ik} and B_{ki} are the Einstein coefficients for absorption and stimulated emission respectively. In Eq. (2), spontaneous emission has been neglected. With this assumption, the rate of change of occupation number due to optical transitions can be written using matrix notation as

$$\underline{\dot{n}}_{opt} = \underline{\dot{n}}_i. \tag{3}$$

Collisional Transitions

Bauer introduced inelastic binary collision processes of the type

$$M_i + M_j \underset{k_\alpha}{\overset{k'_\alpha}{\rightleftarrows}} M_k + M_l \tag{4}$$

where $M_i \ldots\ldots M_l$ may be any energy level of the gas or mixture considered and k_α and k'_α are the forward and backward rates in units of $\text{sec}^{-1}\text{atm}^{-1}$. The net rate of the reaction is given by the difference between forward and backward rate.

The rate of the α^{th} reaction is

$$\dot{\xi}_\alpha = np(k_\alpha x_i x_j - k'_\alpha x_k x_\ell) \tag{5}$$

where ξ_α is the progress variable for reaction α, p is the pressure in atmospheres, n is the total number of molecules and $x_i \ldots x_\ell$ are the mole fractions ($x_i = n_i/n$).

$\dot{\xi}$ is then expanded about a steady-state value assuming a small perturbation. Using the mass action law,

$$\dot{\xi} = npk_\alpha^o x_i^o x_j^o \{[\frac{\partial \ln(pk_\alpha)}{\partial T} - \frac{\partial \ln(pk_\alpha')}{\partial T}](T-T^o) + \sum_m [\frac{\partial \ln(x_i x_j)}{\partial n_m} - \frac{\partial \ln(x_k x_\ell)}{\partial n_m}](n_m - n_m^o)\} \quad (6)$$

where superscripts o refer to the value at the expansion point. Bauer related the first bracket to the reaction heat ΔH_α and used Van t'Hoff's equation to write

$$\frac{\partial \ln k_\alpha}{\partial T} = \Delta H_\alpha / RT^2. \quad (7)$$

The second bracket can be rewritten as

$$\sum_m [\frac{\partial \ln(x_i x_j)}{\partial n_m} - \frac{\partial \ln(x_k x_\ell)}{\partial n_m}] (n_m - n_m^o) = n^{-1}[\frac{n_i - n_i^o}{x_i} + \frac{n_j - n_j^o}{x_j} - \frac{n_k - n_k^o}{x_k} - \frac{n_\ell - n_\ell^o}{x_\ell}]. \quad (8)$$

For multilevel systems a matrix notation is introduced. Let $\underline{\dot{\xi}}_\alpha$ be the vector of $\dot{\xi}_\alpha$; $\underline{n}$ be the vector of $n_i - n_i^o$; $\underline{k}$ be the diagonal matrix $(k_\alpha^o x_i x_j)$ and $\underline{x}$ be the diagonal matrix of all mole fractions.

Further, Bauer constructed a matrix $\underline{\nu}$ with columns corresponding to an individual level, such that $(\nu)_{i\alpha}$ counts the number of times the energy level i occurs more often on the right hand side of the reaction equation α than on the left hand side. This matrix allows one to express all ΔH_α in terms of the energies of one mole of each level, accumulated in the vector u, as $\underline{\bar{\nu}u}$. Equations 6 - 8 now read as

$$\dot{\underline{\xi}}_{\alpha} = -P\underline{k\nu}\ [\underline{x}^{-1}\underline{n}-(\frac{n}{RT^{2}})\underline{u}(T-T^{o})]. \tag{9}$$

Multiplying $\dot{\underline{\xi}}$ by $\underline{\nu}$, the rate of change of the mole numbers due to collision processes is found to be

$$\dot{\underline{n}}_{coll} = -P\underline{\nu k\bar{\nu}}\ [\underline{x}^{-1}\underline{n}-(\frac{n}{RT^{2}})\underline{u}(T-T^{o})] \tag{10}$$

The perturbation term $\dot{\underline{n}}_{coll}$ generates a temperature variation with the rate

$$\dot{T} = -\underline{u}\dot{\underline{n}}_{coll}/(nC_{v}^{\infty}) \tag{11}$$

where $-\underline{u}\dot{\underline{n}}_{coll}$ is the rate of energy flow into translation, and C_{v}^{∞} is the molar heat capacity of translation and all degrees of freedom which share their energy instantly with translation.

Spontaneous Emission

Bauer neglected the effects of spontaneous emission. Spontaneous emission has two experimentally observable effects. At high pressure, since the effect of thermal conduction decreases with increasing pressure, spontaneous emission is a mechanism for transferring energy supplied to the gas by the laser to the cell walls. This effect will parallel thermal conduction and will be important for high gas pressures and long times. At low pressure, spontaneous emission will offer a parallel relaxation path to the slow collisional processes. As a result, the observed relaxation times will be a combination of collisional, spontaneous emission, and wall deexcitation.

The rate of change of occupation number due to spontaneous emission is

$$\dot{n}_s = -\underline{A}n \tag{12}$$

where $\underline{A}$ is the inverse of the radiative lifetime. Including spontaneous emission, Equation (3) becomes

$$\dot{\underline{n}}_{opt} = \dot{\underline{n}}_i + \dot{\underline{n}}_s = -\underline{A}n + \dot{\underline{n}}_i . \tag{13}$$

The total rate of change of occupation number is now

$$\dot{\underline{n}} = \dot{\underline{n}}_{opt} + \dot{\underline{n}}_{coll} \tag{14}$$

Inserting Eq. (13) into Eq. (14) yields:

$$\dot{\underline{n}} - \dot{\underline{n}}_i = \dot{\underline{n}}_{coll} - \underline{A}n. \tag{15}$$

Eq. (15) can be solved numerically. At time $t = 0$, the change in temperature $T-T^o = 0$, then $\dot{\underline{n}}_i$ and $\dot{\underline{n}}_{coll}$ can be determined by using Eqs. (2) and (10) respectively, and then $\dot{\underline{n}}$ can be computed from Eq. (15). At a later time, $t = \Delta t$, a new value for $\underline{n} = \int_{-0}^{+0} \dot{\underline{n}}_{opt} dt + \dot{\underline{n}}\Delta t$ is computed. Also a new value for $T-T^o$ is determined by using Eq. (11). These new values for $T-T^o$ and $\underline{n}$ are used in Eq. (10) to compute a new value for $\dot{\underline{n}}_{coll}$. Eq. (15) is then used to determine a new value for $\dot{\underline{n}}$.

By repeating this procedure again and again for small time changes, the entire temperature evolution can be computed. The pressure change is then computed from the temperature change using the ideal gas law.

Thermal Conduction

In solving the kinetic equations for the spectrophone response, Bauer assumed that thermal conduction to the cell walls is very slow compared to the rate of collisional deactivation. This is true at high pressures. At low pressures of interest here, however, thermal conduction can dominate the measured response.

The equation for heat flow in the test cell when there are sources of heat within it can be written as[10]

$$\frac{\partial\theta(r,t)}{\partial t} = \kappa\left(\frac{\partial^2\theta(r,t)}{\partial r^2} + \frac{1}{r}\frac{\partial\theta(r,t)}{\partial r}\right) + \Theta(r,t) \tag{16}$$

where θ is the difference between the gas and tube temperatures (the tube temperature is assumed to be constant). The rate of heat generation, $H(r,t)$, is assumed to be a product of space and time dependent parts,

$$H(r,t) = f(r)g(t) \text{ so } \Theta(r,t) = \frac{1}{\rho C}H(r,t) = \frac{\kappa}{k}f(r)g(t) \tag{17}$$

where κ is the "thermal diffusivity" and k is the thermal conductivity ($k = \kappa C_v \rho$). The function $g(t)$ is the heat generated by relaxation processes which is equal to $\frac{\partial u(t)}{\partial t}$.

Prior to proceeding further with the solution of Equation (16), a form for $f(r)$ must be assumed. We will assume a uniform radial excitation though some type of a Gaussian distribution across the cell radius might be more appropriate.

For uniform excitation $f(r) = 1$ and

$$\Theta(r,t) = \frac{\kappa}{k}\frac{\partial u(t)}{\partial t}. \tag{18}$$

Equation (16) can then be written as

$$\frac{\partial}{\partial t}[\theta(r,t) - \frac{\kappa}{k}u(t)] = \kappa[\frac{\partial^2\theta(r,t)}{\partial r^2} + \frac{1}{r}\frac{\partial\theta(r,t)}{\partial r}]. \tag{19}$$

Equation (19) can be solved by separation of variables. Let

$$\theta(r,t) = R(r)Q(t). \tag{20}$$

Substituting $\theta(r,t)$ from Equation (20) into Equation (19) and dividing by $R(r)Q(t)$ yields

$$\frac{1}{\kappa R(r)Q(t)}\frac{\partial}{\partial t}[R(r)Q(t) - \frac{\kappa}{k}u(t)] = \frac{1}{R(r)Q(t)}[\frac{\partial^2}{\partial r^2}R(r)Q(t) + \frac{1}{r}\frac{\partial}{\partial r}R(r)Q(t)]. \tag{21}$$

By equating Equation (21) to $-\alpha^2$, the radial equation (the right hand side), has a solution, $R = AJ_o(\alpha r)$, where J_o is Bessel's function and A is a normalization constant to be determined from the boundary conditions.

The boundary conditions require that $\theta = 0$ when r = the cell radius a, hence $J_o(\alpha_m a) = 0$ and α_1, α_2, . . . α_m are zeros of the Bessel function. The radial solution is, then,

$$R_m(r) = \sum_m A_m J_o(\alpha_m r). \tag{22}$$

A_m can be determined[11] to be $2\sum_m \frac{1}{a\alpha_m J_1(\alpha a)}$ so

$$R_m(r) = 2\sum \frac{J_o(\alpha_m r)}{a\alpha_m J_1(\alpha a)}. \tag{23}$$

Substituting for R_m into Eq. (20) yields

$$\theta(r,t) = 2\sum_m \frac{J_o(\alpha_m r)}{a\alpha_m J_1(\alpha_m a)} Q(t). \tag{24}$$

Taking the spatial average of Eq. (24) by integrating across the cell radius,

$$\theta(t) = \frac{2}{a^2}\int_0^a \theta(r,t)dr = 4Q(t)\sum_m \frac{1}{a^2\alpha_m^2} \tag{25}$$

where

$$Q(t) = \frac{1}{4}\,\theta(t)\,\left[\sum_m \frac{1}{a^2\alpha_m^2}\right]^{-1}. \tag{26}$$

The left hand side of Eq. (21) can be written as

$$\frac{\partial}{\partial t}\left[Q(t)\sum_m R_m(r) - \frac{\kappa}{k}u(t)\right] = -\kappa\sum_m \alpha^2{}_m R_m(r)Q(t). \tag{27}$$

Averaging over r,

$$\frac{d}{dt}\left[\sum_m \frac{4}{a^2\alpha_m^2}Q(t) - \frac{\kappa}{k}u(t)\right] = -\frac{4\kappa}{a^2}\,Q(t). \tag{28}$$

Substituting for Q(t) into Eq. (28)

$$\frac{d\theta}{dt}(t) = \frac{\kappa}{k}\frac{du}{dt}(t) - \frac{\kappa\theta}{a^2}(t) \tag{29}$$

If we substitute for κ and $\frac{du}{dt}$, Equation (29) becomes

$$\frac{d\Theta(t)}{dt} = \frac{1}{nC_v^\infty}\,P\nu k\bar{\nu}\,\left[\underline{x}^{-1}\underline{n} - \left(\frac{n}{RT^2}\right)\underline{u}(T-T^o)\right] - \frac{kRT}{PC_v^\infty}\,\frac{\theta(t)}{a^2}\left[\sum_m \frac{1}{a^2\alpha_m^2}\right]^{-1}. \tag{30}$$

Eq. (30) consists of two terms. The first one is due to collisional processes given earlier in Eq. (11) and it is directly proportional to

the pressure. The second one is due to thermal conduction and it is inversely proportional to the pressure.

It is clear from Eq. (30) that at high pressure the thermal conduction term can be neglected and the rate of change of temperature is mainly due to collisional processes, while at low pressure thermal conduction can not be neglected. Eq. (30) can be solved numerically.

Bass and Yan[6] have modified Bauer's theory by including thermal conduction and wall collisions in the theory. They also used Bauer's matrix notation to solve for the kinetic equations of the spectrophone. Our solution of Eq. (30) using numerical integration is compared to the Bass and Yan result in Figure 3.

Effect of Wall Collisions

According to Margottin-Machou, Dogonette, and Henry[12], the effective relaxation rate $\beta(= \frac{1}{\tau_{eff}})$ can be written as

$$\beta = k_c + k_w + \pi_p \tag{31}$$

where k_c is the collisional deactivation rate, k_w is the rate of deexcitation by the walls and π_p is the rate of deactivation by spontaneous emission (including trapping). They further show that for a long narrow tube,

$$k_w = \mu^2 (D/R^2) \tag{32}$$

where D is the diffusion coefficient, R is the cell radius, and μ is a solution of $\mu J_1(\mu) = hJ_o(\mu)$, where $h = (R\bar{\nu}/2D)(a/2-a)$, $\bar{\nu}$ is the

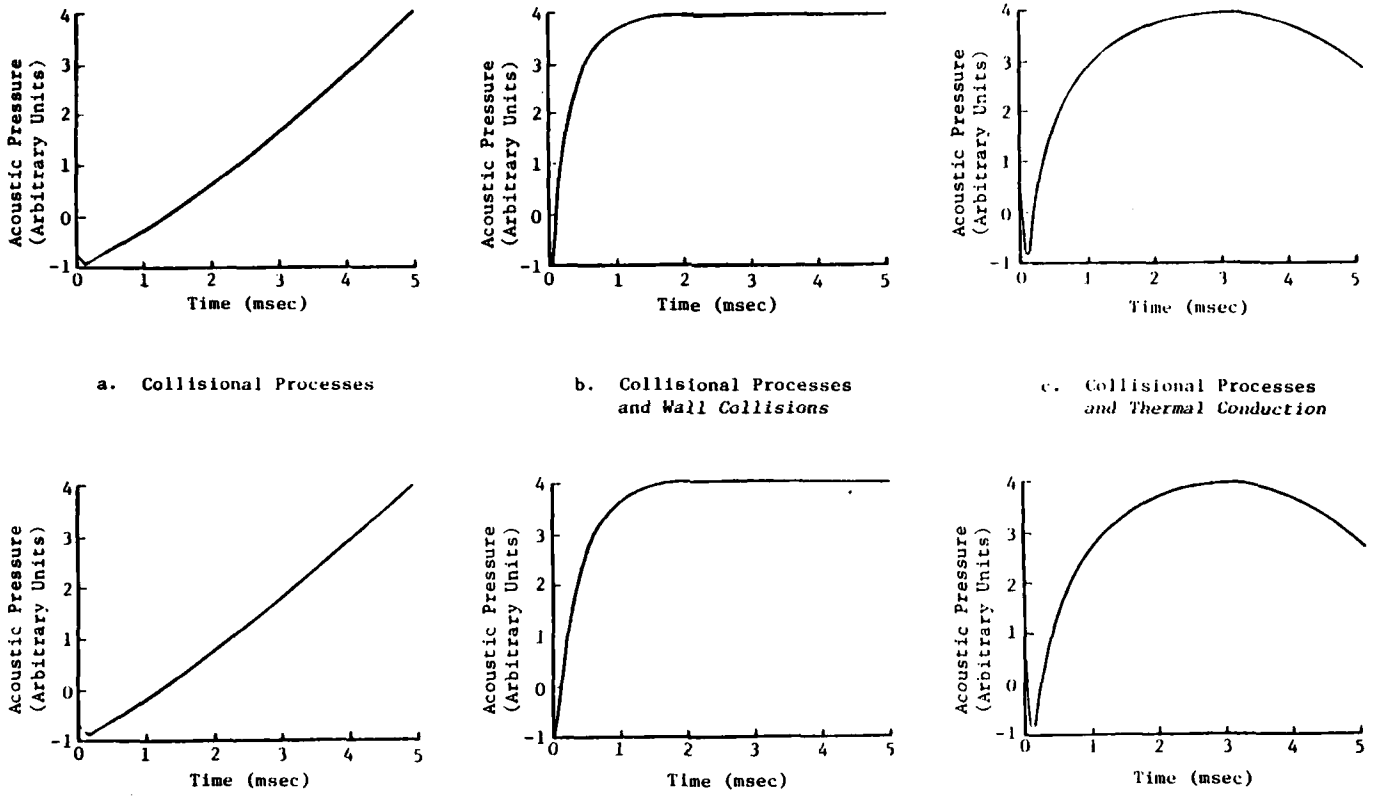

Figure 3. Comparison of Eq. (30) (Lower Curves) and Bass and Yan's Result (Upper Curves).

mean speed of molecules, and a is the probability of deexcitation during a collision with the cell walls. The ratio R/h is the minimum distance a molecule must travel close to a wall before being deexcited $\cong \lambda/a$ where λ is the mean free path. The diffusion coefficent D is pressure dependent so we will write $D_o = DP$.

Margottin-Machou, Dogonette, and Henry found that for pressures of 1 Torr and above, μ approaches a limiting value of 2.4. For pressures of interest in this work μ varies from 2.4 - 3.6. Changing from 2.4 to 3.6 has no significant effect on the shape of the pressure wave, so Eq. (31) was written as

$$k_w = (2.4)^2 D_o / R^2 P \tag{33}$$

where D_o is the kinetic self-diffusion coefficient.

Acoustic Effect

As the incoming radiation propagates down the axis of the tube, absorption of radiation by the gas decreases the intensity in accordance with Beer's Law, $I = I_o e^{-\mu z}$. Since the absorbed energy in any small section of the tube differs from that in the next section, the resulting temperature and pressure rise will decrease down the tube axis. A pressure gradient down the tube will, of course, give rise to a net force causing gas near the entrance window to expand into the lower pressure regions further from the entrance window. This expansion is observed as a longitudinally propagating acoustic wave (superimposed upon a uniform pressure change). For the acoustic wave, the effect of the boundaries is

important. Boundaries cause reflections which must be added to the wave developed by the source to give the total pressure. To determine the total pressure at any point, we will use a Green's function approach and the method of images.

According to Morse and Feshbach[13] the solution to the one-dimensional scalar wave equation is

$$p(x,t) = \int_0^t dt_o \int_0^x dx_o G(x,t|x_o,t_o)T(x_o,t_o) \tag{34}$$

where x_o represents the source point, t_o represents the time when the source is applied, x represents the observation point, where the field is measured, t represents a time later than when the source was applied at x_o, p is the presssure at the observation point, T is the temperature which describes the source density as a function of space and time, and G is the Green's function describing the effect of the source as it propagates away from x_o in the course of time.

To apply the method of images consider the test cell as a cylindrical tube of length L as shown in the following diagram.

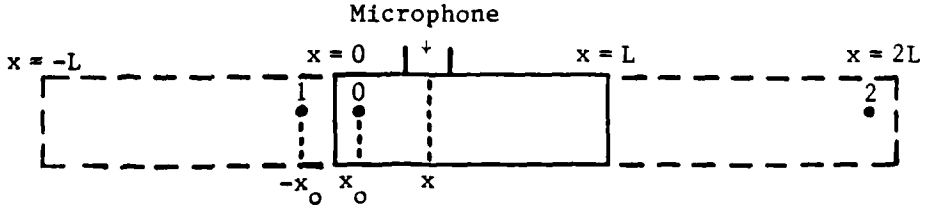

Figure 4. A Sequence of Images of Source.

The method of images is applied in a stepwise fashion, by considering each boundary x = 0 and x = L in turn. Disregarding the x = L boundary, an image is introduced at $x = -x_o$. Disregarding x = 0, an image is introduced at $x = 2L - x_o$. This process could continue indefinitely, leading to an infinite number of images, since there are an infinite number of reflections for any ray started at the source. Each image corresponds to one of these reflections.

The number of images required will depend on the distance travelled by sound inside the gas sample during the time of interest. For SF_6, the sound travels 40 cm in the 4 msec typically of interest in our experiments. Since the length of the test cell is 50 cm, this implies that only one image at $x = -x_o$ is needed.

The one dimensional Green's function for our problem is given by[13]

$$G(x,t|x_o,t_o) = 2C\pi[1-u(\frac{|x-x_o|}{C} - (t-t_o))] \tag{35}$$

where

$$u[\frac{|x-x_o|}{C} - (t-t_o)] = \begin{cases} 1 \text{ when } \frac{|x-x_o|}{C} > (t-t_o) \\ 0 \text{ when } \frac{|x-x_o|}{C} < (t-t_o) \end{cases} \tag{36}$$

These conditions for u give an upper limit for $x_o \leq x+C(t-t_o)$ and a lower limit for $x_o \geq x-C(t-t_o)$. For times less than $t = \frac{x}{C}$, there is no need for the image so

$$p(x,t) = 2\pi C \int_0^{t<\frac{x}{C}} dt_o \int_{x_o = x-C(t-t_o)}^{x_o = x+C(t-t_o)} dx_o T(x_o,t_o) \tag{37}$$

After a time $t = \frac{x}{C}$ up to $t = (L-x)/C$, there is one image to consider located at $-x_o$ so

$$p(x,t) = 2\pi C \int_0^{t=\frac{x}{C}} dt_o \int_{x_o=x-C(t-t_o)}^{x_o=x+C(t-t_o)} dx_o T(x_o,t_o) + 2\pi C \int_{t=\frac{x}{C}}^{t} dt_o \int_{x_o=0}^{x_o=x+C(t-t_o)} dx_o T(x_o,t_o)$$

$$+ 2\pi C \int_{t=\frac{x}{C}}^{t} dt_o \int_{x_o=x-C(t-t_o)}^{0} dx_o T(x_o,t_o). \qquad (38)$$

To solve for $p(x,t)$ we need to determine $T(x_o,t_o)$. $T(x_o,t_o) = e^{-\mu x_o} T(t_o)$ where μ is the absorption coefficient for the gas. In order to determine $T(t_o)$ the standard attenuation mechanisms must be considered. These losses are caused by viscosity, thermal conductivity, mass diffusion, and vibrational and rotational relaxation. In addition, there are losses associated with sound propagation inside the tube. When sound propagates through polyatomic gases the compressions and rarefactions involve a redistribution of energy between the various modes of excitation; this includes vibrational and rotational modes. At sufficiently high frequencies, the period of fluctuation becomes shorter than the time required for the redistribution of energy into various modes. When this occurs the compressions and rarefactions are no longer reversible and attenuation results. Since rotational energy levels are closely spaced near room temperature for SF_6, a single relaxation time can be used[14] to describe rotational relaxation. For vibrational attenuation, the coupling between v-t and v-v processes complicates the problem[15,16] greatly; however, SF_6 has properties which simplify the problem. SF_6 has

many vibrational levels which are excited even at low temperatures ~300K but, the lowest level deexcites much slower than the others. This lowest level gating makes it possible to characterize SF_6 vibrational relaxation with one relaxation time[16].

The attenuation coefficient was determined by using a computer program developed by Shields which is described in Reference 17. $T(t_o)$ can be determined by the following steps:

1. Solve Eq. (30) numerically, $T(t) = \theta(t)$ can be determined.
2. Fourier transform $T(t)$ to get $T(\omega)$.
3. Compute the attenuation coefficient α as indicated earlier for all frequencies of interest.
4. Compute $\tilde{T}_{t_o}(\omega) = T(\omega)10^{-x\alpha(\omega)/20}$.
5. Inverse $\tilde{T}_{t_o}(\omega)$ to get $T(t_o)$, and then substitute the value of $T(t_o)$ into Eq. (38) and solve for $p(x,t)$.

Test of the Computer Program

To solve Eq. 30 numerically, a computer program was developed. As a first test, the output of the program was examined for pressures of 1 torr and 2 torr. At these pressures, collisional processes dominate the results. Since the rate of collisional deexicitation (one over the relaxation time) is directly proportional to pressure, the two curves should overlap when the 2 torr curve is plotted on a scale covering 1/2 the time. The result of this test is shown in Figure 5. There is a slight difference due to the finite time increment used for the numerical integration. This difference is not considered significant.

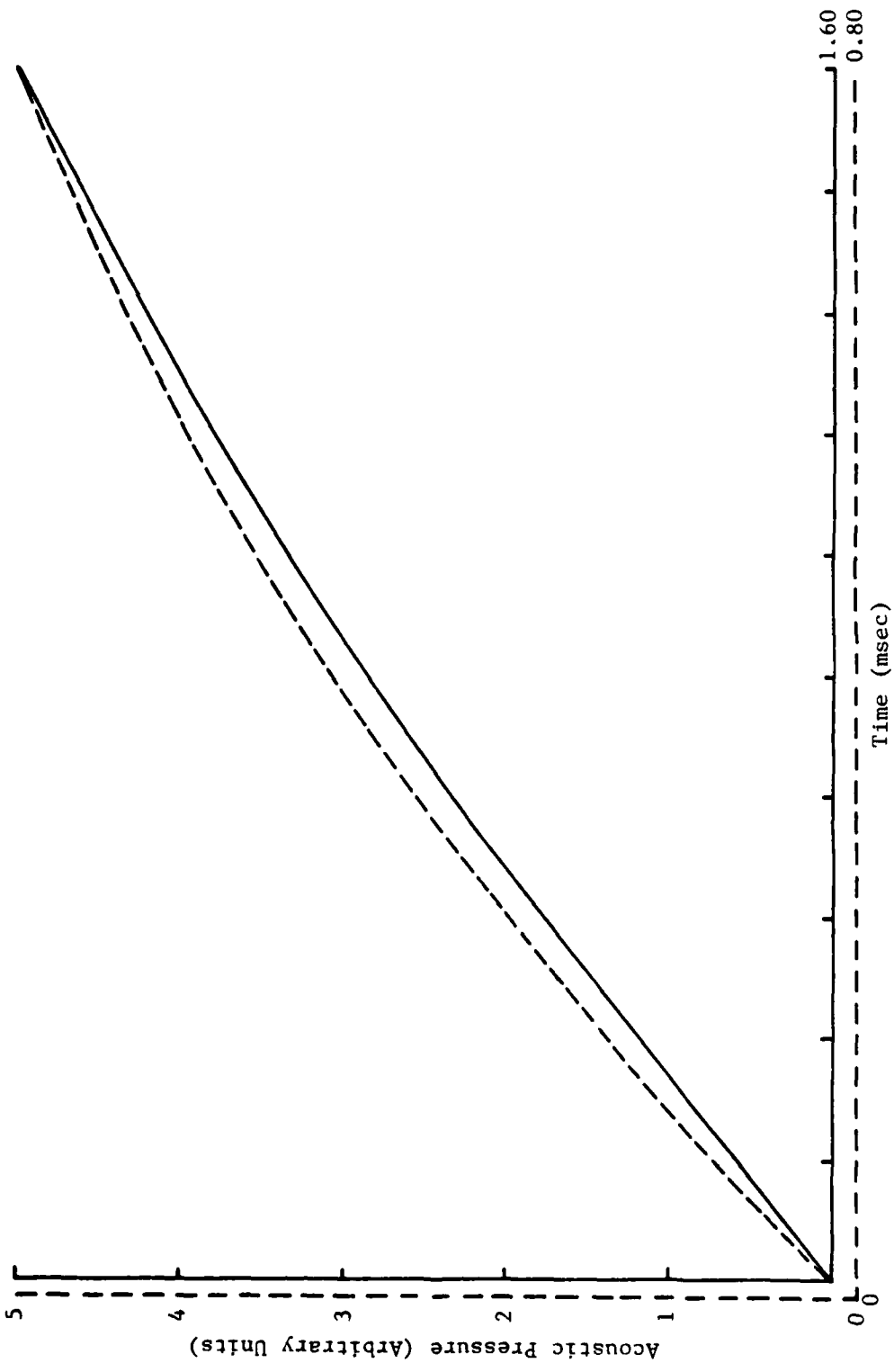

Figure 5. Computed Waves at High Pressures. — for pressure = 1 torr; -- for pressure = 2 torr.

Figure 6 shows computed curves at intermediate pressures (0.8 and 0.4 torr) where thermal conduction is important as well as collisional energy transfer. The long term return of the pressure back to equilibrium reflects thermal conduction to the tube walls. From Fig. 6, the thermal conduction decay time for a pressure of 0.8 torr is two times larger than that for a pressure of 0.4 torr. This agrees with the theory which suggests that thermal conduction decay time (one over the rate) is linearly proportional to the pressure.[6]

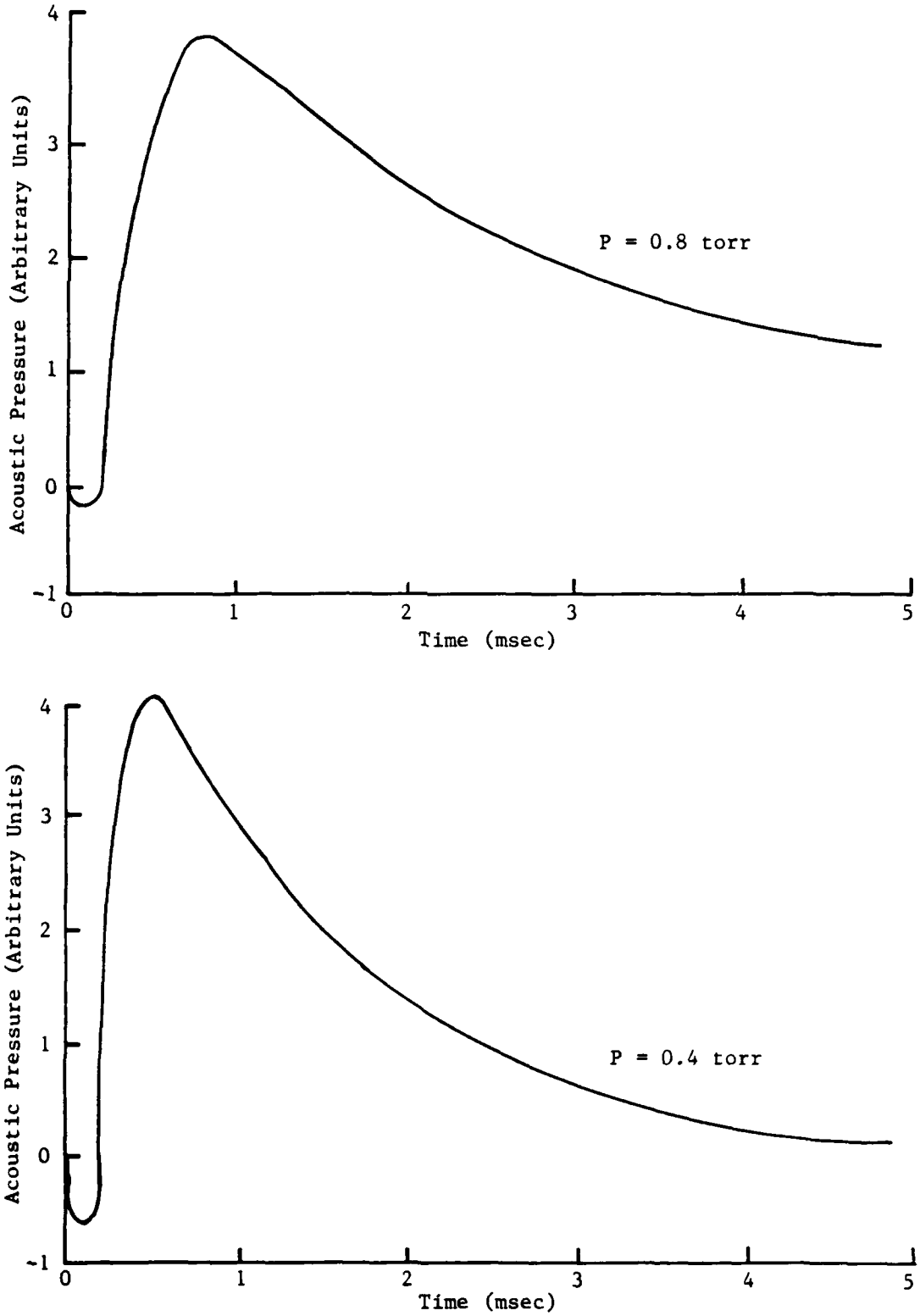

Figure 6. Computed Waves at Intermediate Pressures.

CHAPTER 4

Experimental Result

A typical pressure waveform obtained in this experiment is shown in Figure 7. This figure shows the variation of pressure amplitude (in arbitrary units) versus time. Energy deposited in the gas by a short laser burst appears first as a small perturbation in the population of vibrationally excited states. Following a sufficient number of collisions, the excess energy will redistribute over internal and translational modes. Changes in temperature and pressure will result as the energy cascades down through the manifold of vibrational states. The resulting pressure evolution will appear as shown in Figure 7. Figure 7 also shows that the pressure decreases (positive pressure is down) for very short times. Since there is a net gain of energy by the gas, on a longer time scale, the pressure will go positive. For even longer times, the pressure will depend on acoustic effects, spontaneous emission, and thermal conduction to the cell walls which take the system back to equilibrium.

As the gas pressure is decreased the amplitude of the pressure wave becomes smaller down to 200 mTorr. At this point, the sign of the pressure change reverses (becomes negative) and the amplitude begins to increase as the pressure is decreased further as shown in Fig. 8.

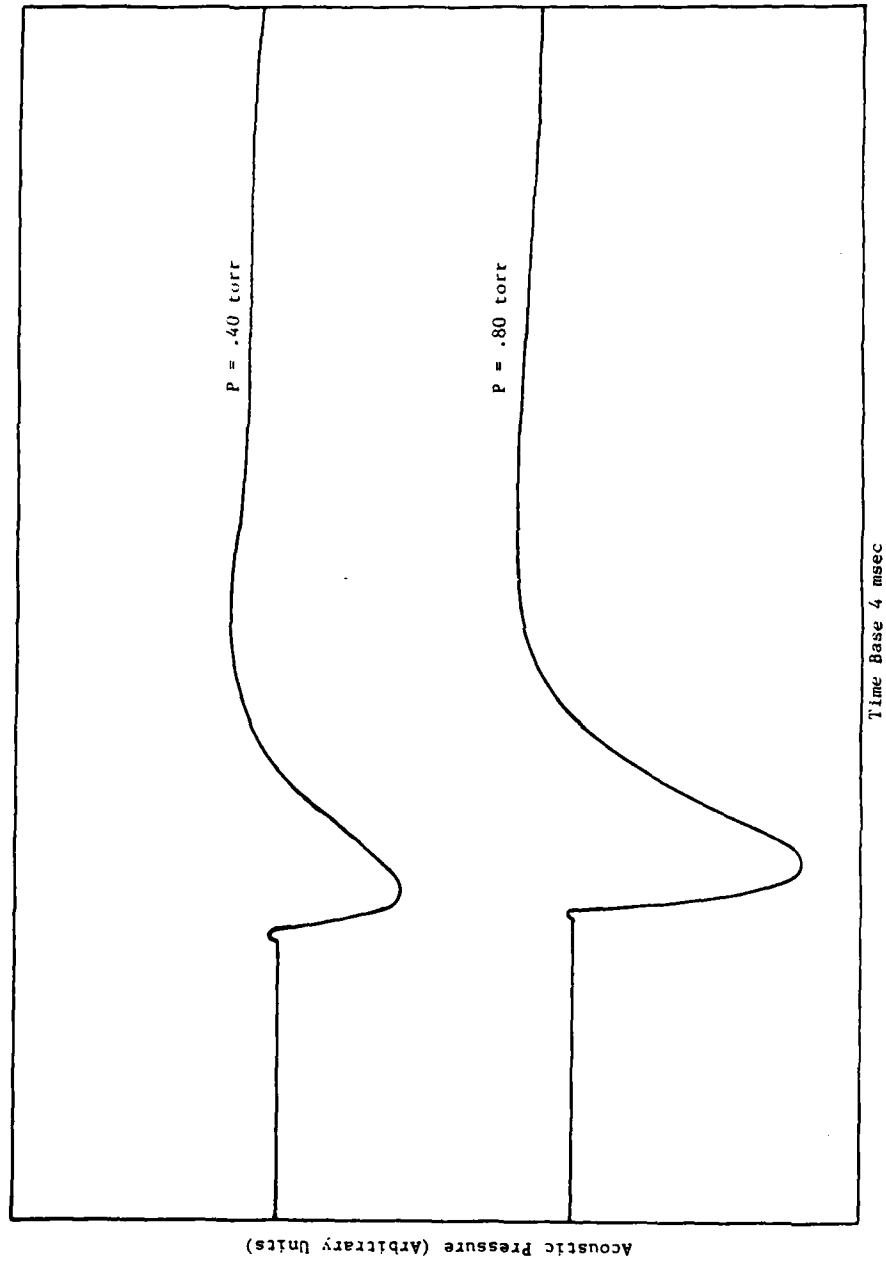

Figure 7. Typical Pressure Waveform (Positive Pressure is Down).

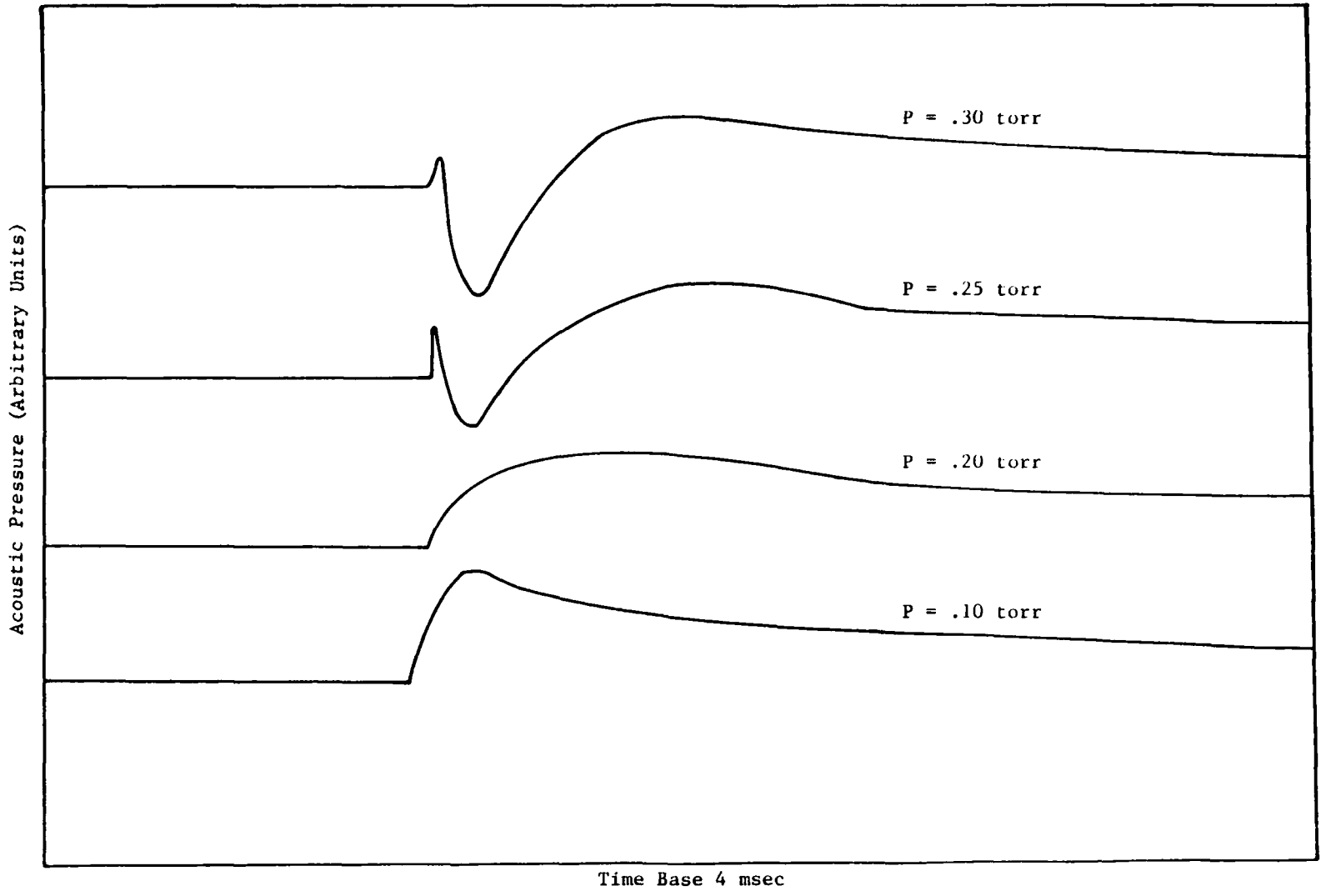

Figure 8. Change in Sign of Pressure Amplitude as the Gas Pressure is Decreased (Positive Pressure is down

The form of the differential equations in the preceeding Chapter suggests that the pressure will vary as a sum of exponential increases and decays, i.e.,

$$P = P_o e^{-t/\tau},$$

where P_o is the equilibrium pressure and τ is some effective decay time which will change with time. By plotting the pressure amplitude on a semilog scale versus time, rise times and decay times for specific time intervals can be determined at different values of pressures as shown in Fig. 9. Table I shows the experimental rise times and decay times for the positive pressure amplitude (intermediate pressure regime). It can be seen from this table that the relaxation times are only weakly dependent on pressure. Table 2 shows the rise time and decay time for the negative pressure amplitude (below 200 mTorr). At these pressures both times are pressure dependent.

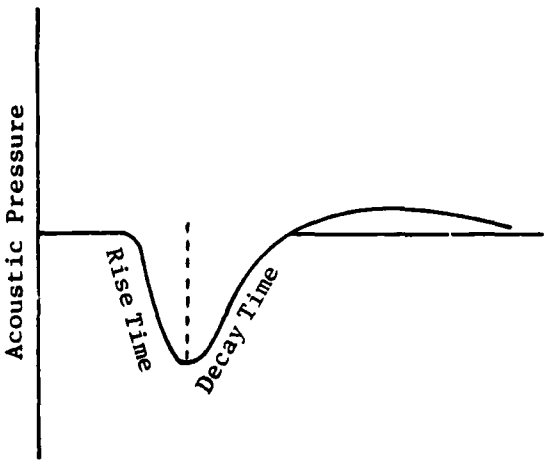

Figure 9. The Rise Time and Decay Time (Positive Pressure is Down).

TABLE I

Pressure (mTorr)	Risetime (msec)	Decay time (msec)
1000	0.078	.295
800	0.078	.280
600	0.078	.280
400	0.080	.270
300	0.082	.150

TABLE II

Pressure (mTorr)	Risetime (msec)	Decay time (msec)
200	.280	1.98
160	.132	1.84
100	.112	1.44
70	.096	1.37
30	.094	1.18

CHAPTER 5

Interpretation and Conclusions

The SF_6 molecule has 15 vibrational degrees of freedom and six fundamental modes.[18] It strongly absorbs 10.6 μm CO_2 laser radiation[19] because most of the absorbing molecules are in the ground or lowest excited vibrational state. To interpret the experimental data of Figs. 7 and 8 first consider the energy level diagram of SF_6. Fig. 10 shows a few of the low-lying levels.[20]

The first experimental observation to be considered is the decrease in gas temperature and pressure immediately following the input of energy from the laser. This seems to violate laws of thermodynamics. To understand this effect, examine the result of competing energy transfer processes which take place in the gas. Ignore, for now, effects of thermal conduction to walls and spontaneous emission.

The laser excites the ν_3 mode which becomes over populated. Absorption from the low-lying ν_6 level to $\nu_3 + \nu_6$ level can also occur with the same result; an increase in ν_3 population. Likewise, a molecules in the level $\nu_3 + \nu_6$ can be excited to $2\nu_3 + \nu_6$. From Fig. 10 it can be seen that the easiest way for the excited molecules at level ν_3 to reach equilibrium is to undergo a v-v transfer to an energy level slightly higher in energy (denoted by reaction 1). The energy deficit in this reaction must come from somewhere. It comes from translation; the gas cools. As time progresses, energy in the upper vibrational levels cascades downwards returning energy to translation resulting in heating.

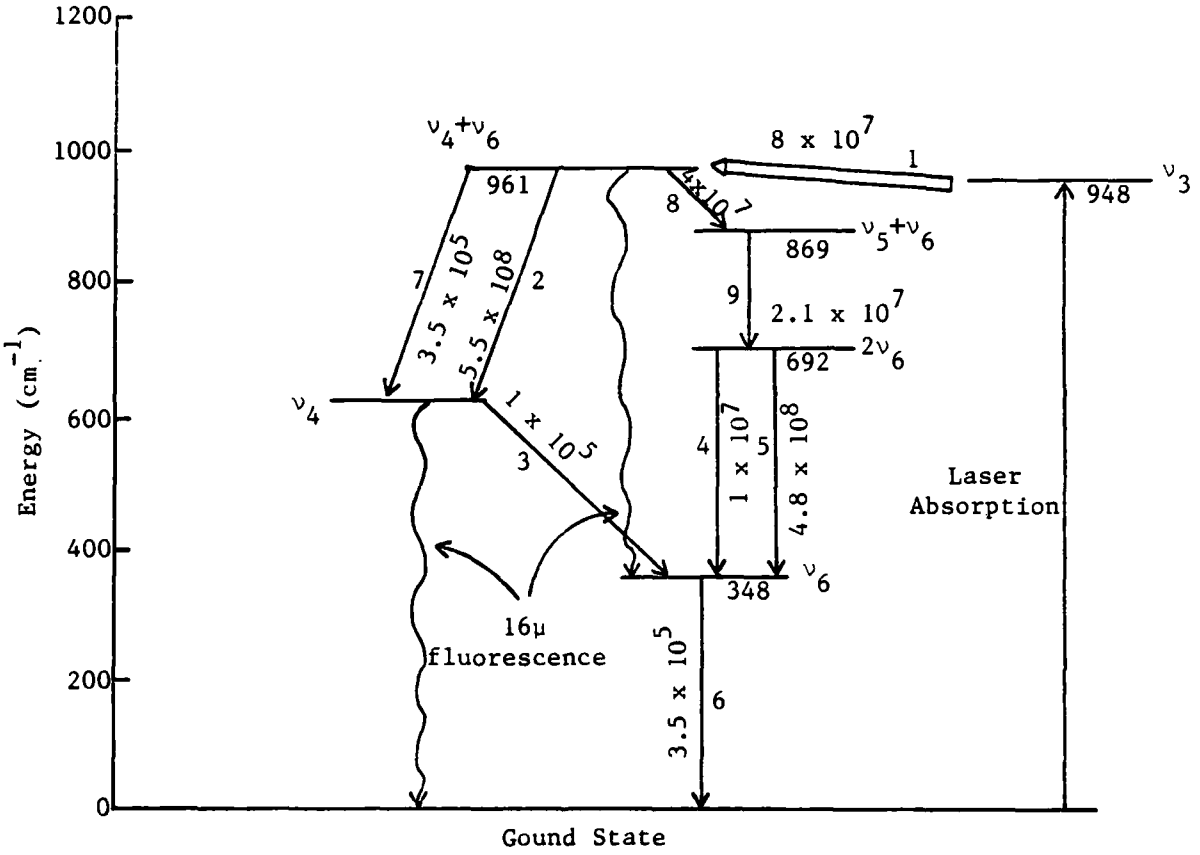

Figure 10. Partial Vibrational Energy Level Diagram for SF_6.

Now consider what will happen when the pressure is so low that thermal conduction and spontaneous emission are faster than the transfer of energy to translation but slower than the initial v-v process which causes the gas to cool. The result, shown in Fig. 8, is that the gas initially cools but rather than transferring excess energy to translation, it is transferred to the tube walls. Since the test cell has a large specific heat, one observes only cooling.

Figure 11 shows computed curves for a sequence of pressures (0.30, 0.25, 0.20 and 0.10 torr). From this figure it can be seen that as the pressure is decreased the amplitude decreases until the pressure reaches 0.2 torr where the amplitude changes sign (becomes negative) and starts increasing. This behavior agrees with the experimental observation shown in Figure 8.

Referring back to Figure 7, the second experimental observation is that in the intermediate pressure regime, the curve does not return to zero after decaying; it overshoots below equilibrium. This is due to acoustic effects which have not yet been considered. Figure 12 shows the two curves computed for the same conditions as in Figure 6 after including acoustic effects. It can be seen from this figure that the acoustic effects cause the curve to go below equilibrium, returning slowly to equilibrium on a longer time scale.

It can be seen from Figure 7, also, that the time from the peak of the curve to the point where it goes below zero is 0.40 msec for a pressure of 0.4 torr and 0.48 msec for a pressure of 0.80 torr. Another

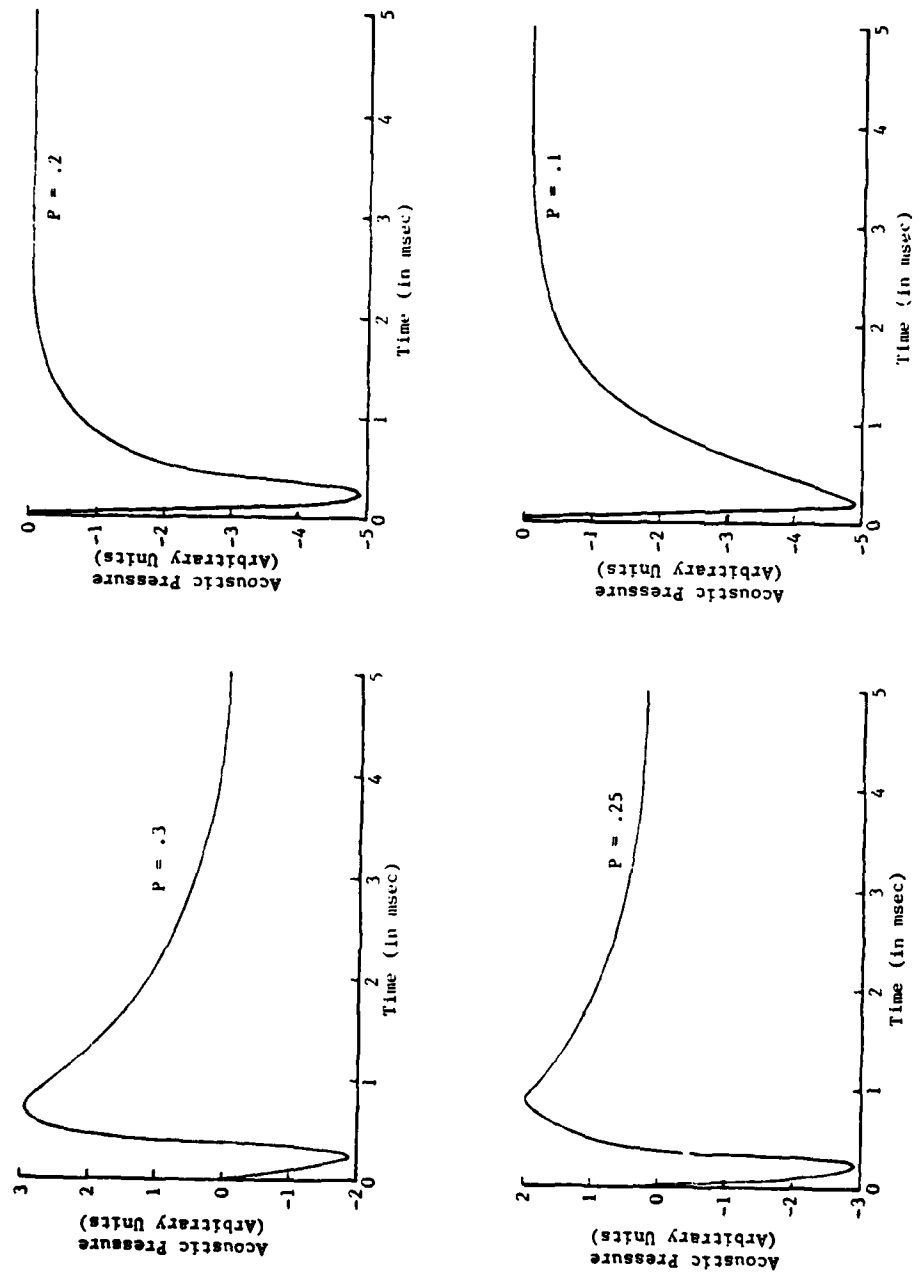

Figure 11. Computed Curves for Sequence of Pressures.

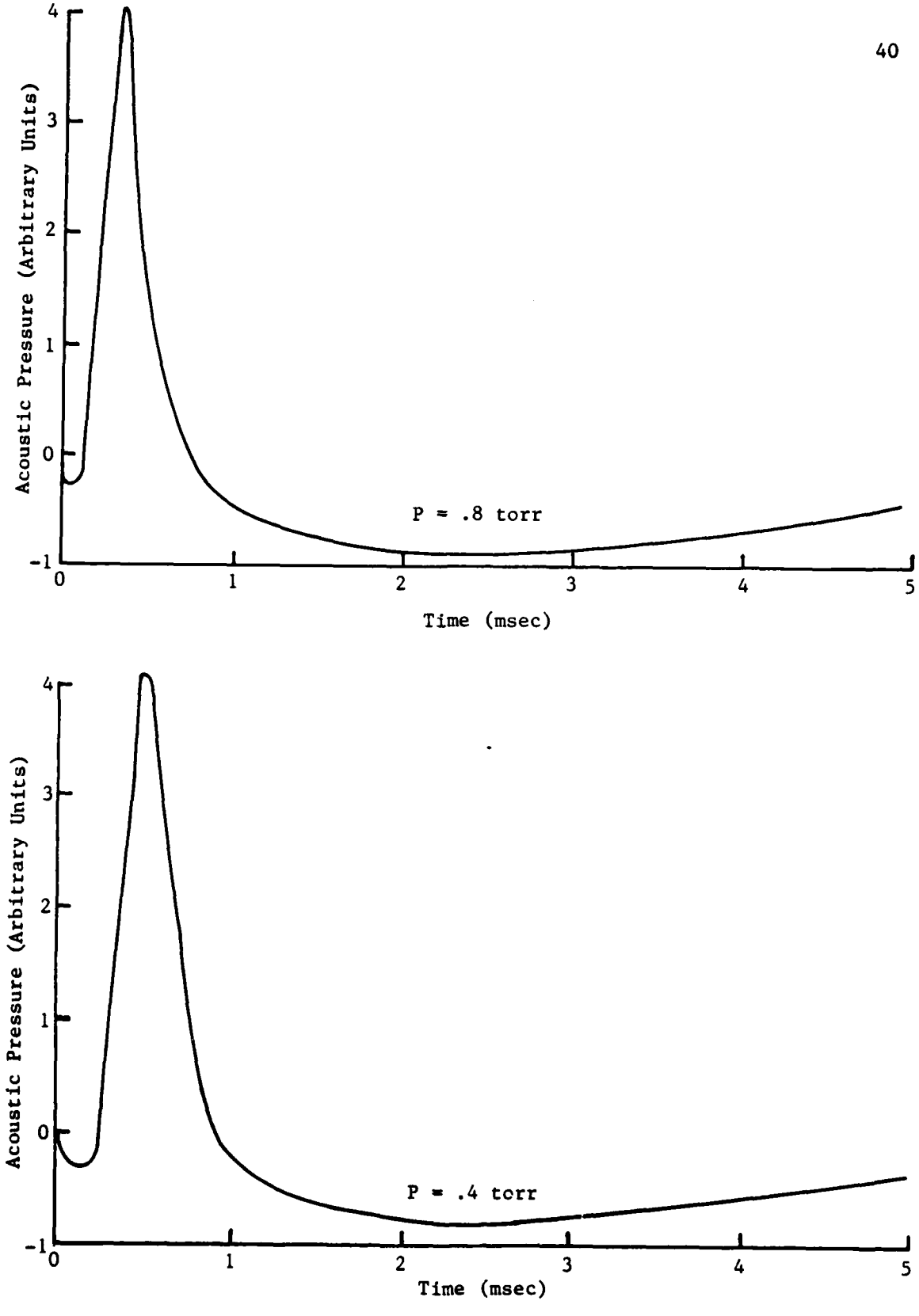

Figure 12. Acoustic Effects at Intermediate Pressure Curves.

feature of this figure is that the ratio between the negative part of the curve to the positive part is 1/5 and 1/4 for pressures of 0.8 and 0.4 torr, respectively. By assuming an effective radius of 0.06 cm, the computed curves in Figure 13 fit experimental data quite well. Figure 14 compares experimental data with computed points for the low pressure regime (0.1 torr). From Figures 13 and 14, it can be seen that the computed curves agree well with the experimental observations.

Figure 15 shows two computed curves at low pressure (0.05 torr). The dashed curve shows the pressure wave when spontaneous emission is included. The other curve shows the pressure wave when spontaneous emission is excluded. It can be seen from this figure that the dashed curve has the more rapid decay time; spontaneous emission offers a parallel pathway for deexcitation processes at low pressures.

From the foregoing, we concluded that the experimental measurements can be reproduced theoretically by assuming a relaxation scheme which connects the various modes of SF_6 collisionally to translation with rate constants for the various processes taken from other measurements or guessed. The rate constants were varied to best fit the data in Figure 7 and 8 with the constraint that ultrasonic and laser fluorescence relaxation times for this same set of rates agree with independent experimental measurements of those quantities. This same procedure was repeated for other energy transfer pathways until best agreement between computed and measured pressure waves was obtained. The final reaction scheme assumed is given in Figure 10.

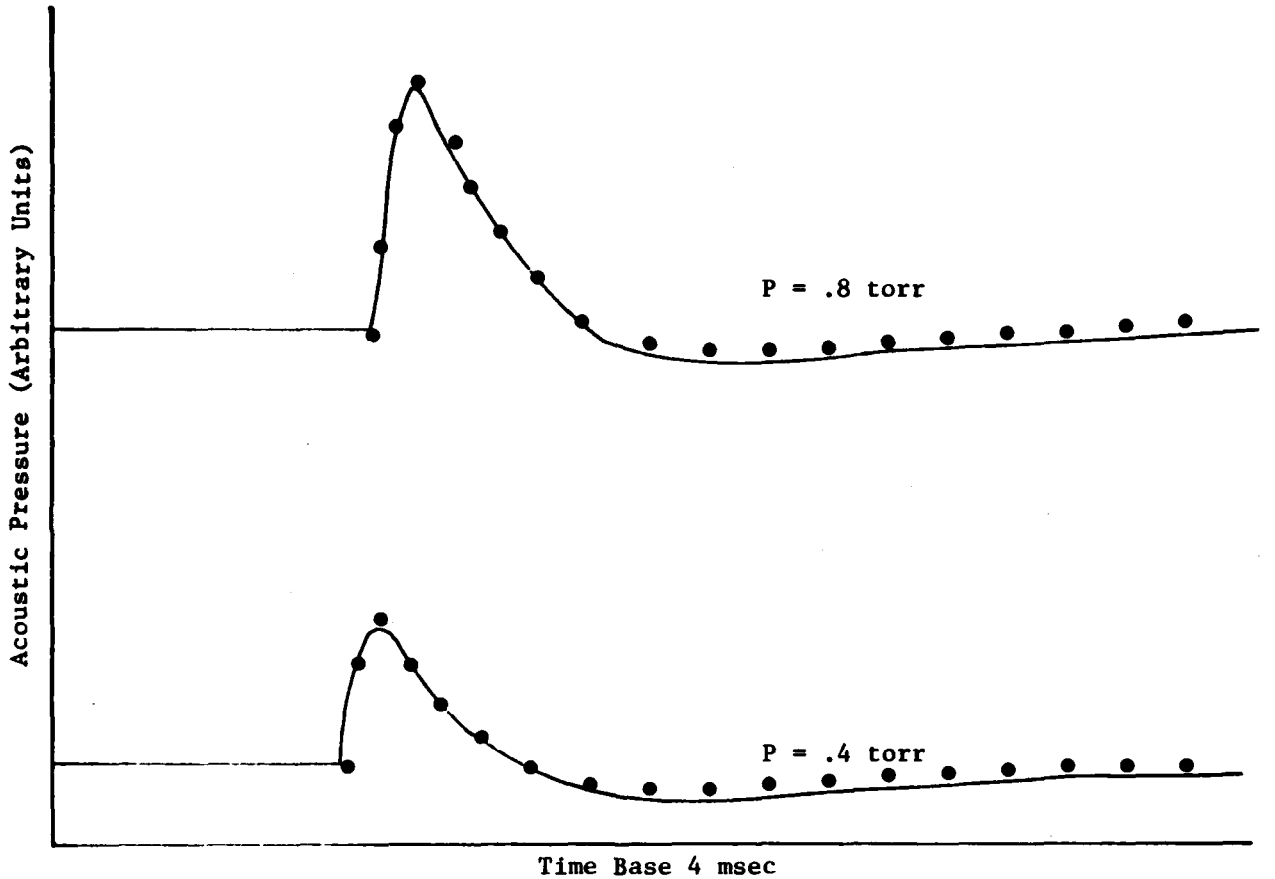

Figure 13. Fitting of Experimental Data with Computed Points. ——, Experimental Data; ●●●●●, Computed Points.

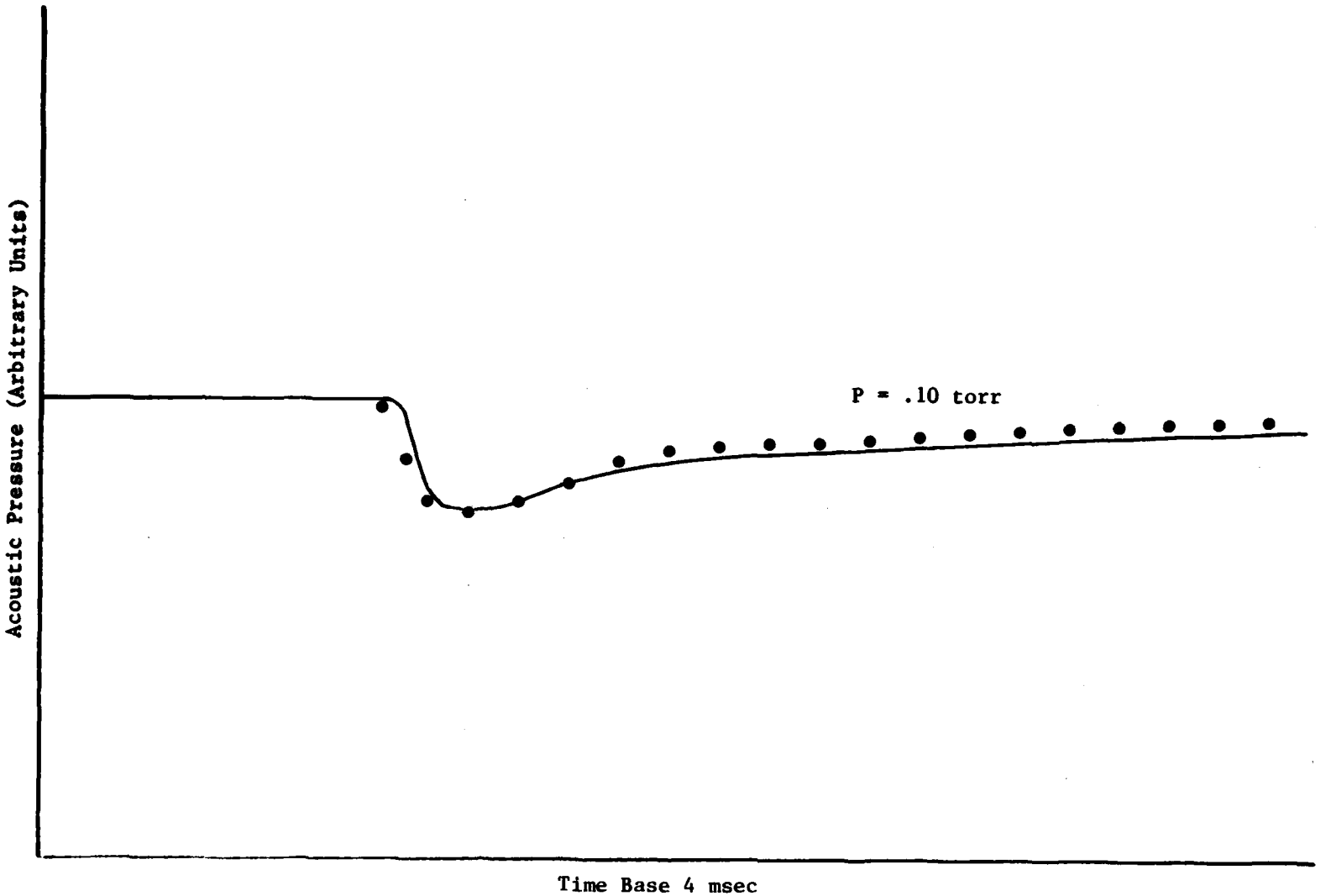

Figure 14. Fitting of Experimental Data with Computed Curve (Low Pressure Regime). ———, Experimental Data; ●●●●●, Computed Points.

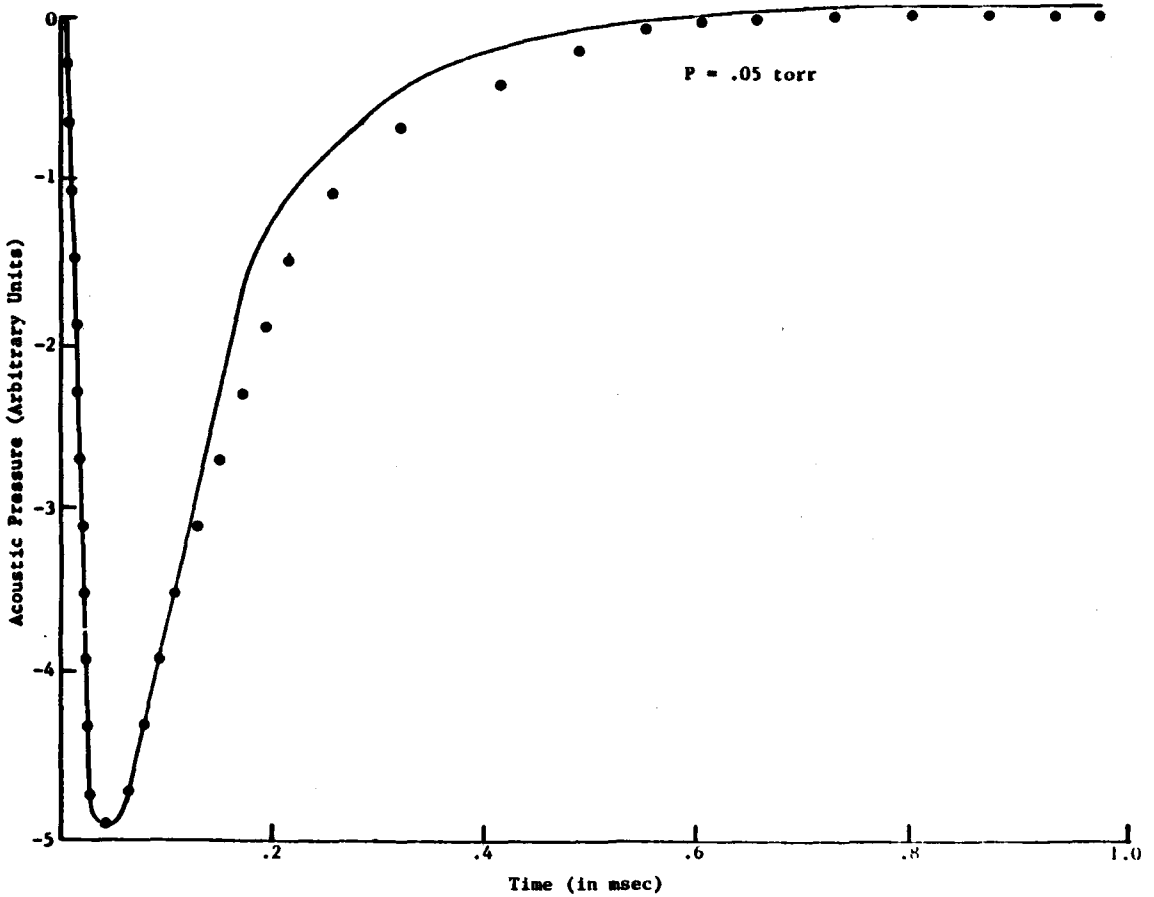

Figure 15. The Effect of Spontaneous Emission at Low Pressure. ——, with spontaneous emission; ●●●●, without spontaneous emission.

REFERENCES

1. A.G. Bell, "Production of Sound by Radiant Energy," Am. J. Sci. 21, 463-490 (1881).

2. T.L. Cottrell and J.C. McCoubrey, Molecular Energy Transfer in Gases, (Butterworths, London, 1961), pp. 64-73.

3. G. Gorelik, Dokl. Akad. Nauk SSSR 1946, 54, 779.

4. M. Heutz-Aubert and R. Tripodi, "Rate Equations for the Vibrational Relaxation of CO_2-N_2 or CO_2-NobleGas Mixtures - Application to Comparison of Spectrophone Data with Result from other Experimental Techniques," J. Chem. Phys. 55, 5724-5734 (1971).

5. T. Aoki and M. Katayama, "Impulsive Optic-Acoustic Effect of CO_2, SF_6 and NH_3 Molecules," Jpn. J. Appl. Phys. 10, 1303-1310 (1971).

6. Henry E. Bass and Hai-Xing Yan, "Pulsed Spectrophone Measurements of Vibrational Energy Transfer in CO_2," J. Acoust. Soc. Am. 74 (6), 1817-1825 (1983).

7. Hans-Jorg Bauer, "Sonet Lumiere or the Opto-Acoustic Effect in Multilevel Systems," J. Chem. Phys. 57, 3130-3145 (1972).

8. R.D. Bates, Jr., J.T. Knudtson, and G.W. Flynn, "Energy Transfer Among Excited Vibrational States of SF_6," Chem. Phys. Lett., 8 (1), 103-107 (1971).

9. Richard D. Bates, J.R. George, W. Flynn, and J. Thomas Knudtson, "Laser-induced 16 Fluorescence in SF_6: Acoustic Effects," J. Chem. Phys. 53 (9), 3621-3631 (1970).

10. I.N. Sueddon, Fourier Transforms, (McGraw Hill Co., LOCALE, DATE), p. 202.

11. H.S. Carslaw and J.C. Jaeger, Conduction of Heat in Solids, (Oxford Univ. Press, London, 1959), p. 198.

12. M. Margottin-Maclou, L. Doyenetti, and L. Henry, "TITLE," Applied Optics 10, 1768-1780 (1971).

13. P.M. Morse and H. Feshbach, Methods of Theoretical Physics, (McGraw Hill, LOCALE, DATE), p. 843.

14. H.E. Bass, L.C. Sutherland, J. Piercy, and L. Evans, "Absorption of Sound by the Atmosphere," Physical Acoutics, Vol. XVII (Academic Press, LOCALE, 1984), PP. __.

15. H.J. Bauer, F.D. Shields, and H.E. Bass, "TITLE," J. Chem. Phys. 57 (11), 4624 (1972).

16. H.E. Bass, "Final Report on an Experimental Study of Vibrational Relaxation of UF_6, WF_6 and MoF_6," JOURNAL VOL. (#), PAGES (DATE).

17. F.D. Shields, K.P. Lee, and W.J. Wiley, "TITLE," J. Acoust. Soc. Am. 37, 724 (1965).

18. G. Herzberg, Infrared and Raman Spectra of Polyatomic Molecules, (Van Nostrand, New York, 1945), p. 337.

19. W. Fuss and J. Hartmann, "TITLE," J. Chem. Phys. 70, 5468 (1979).

20. James Cohen, "Vibrational Relaxation of SF_6," 29th G.E.C., (1976).

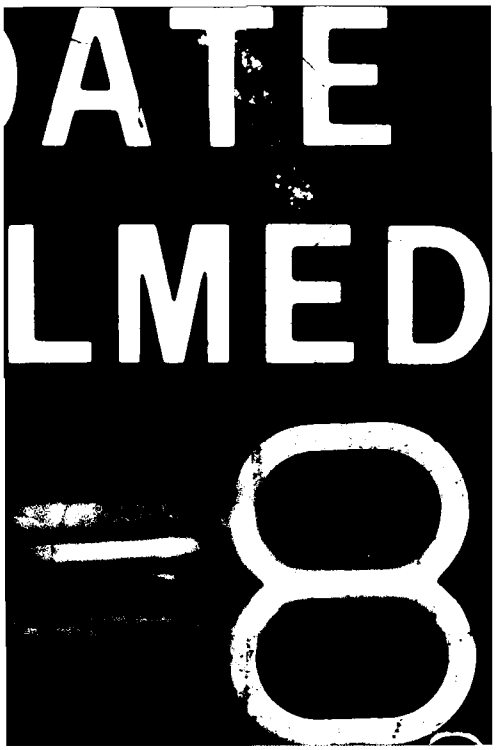
ATE
LMED
8